Natural Convection from a Horizontal Cylinder of Elliptic Cross Section in Saturated Porous Media Using a Thermal Non-Equilibrium Model

CHING-YANG CHENG
Department of Mechanical Engineering
Southern Taiwan University of Technology
1, Nantai Street, Yungkang 71005
TAIWAN

Abstract: - This work uses a thermal non-equilibrium model to study the natural convection heat transfer near a horizontal cylinder of elliptic cross section with constant wall temperature in a fluid-saturated porous medium. A coordinate transformation is used to obtain the nonsimilar governing boundary layer equations. The transformed governing equations are then solved by the cubic spline collocation method. Results for the local Nusselt numbers are presented as functions of the porosity scaled thermal conductivity ratio, the heat transfer coefficient between the solid and fluid phases, and the aspect ratio when the major axis of the elliptical cylinder is vertical (slender orientation) and horizontal (blunt orientation). An increase in the porosity scaled thermal conductivity ratio or the heat transfer coefficient between the solid and fluid phases tends to increase the heat transfer rates. Moreover, the heat transfer rates of the elliptical cylinder with slender orientation are higher than those with blunt orientation.

Key-Words: - Thermal non-equilibrium model, Natural convection, Porous medium, Elliptic cylinder, Cubic spline collocation method, Coordinate transformation.

1 Introduction

Heat and mass transfer driven by thermal and solutal buoyancy forces in a fluid-saturated porous medium is of great importance in geophysical, geothermal and industrial applications, such as the extraction of geothermal energy and the migration of moisture through air contained in fibrous insulations.

Merkin [1] presented the similarity solutions for natural convection heat transfer on a horizontal cylinder in a saturated porous medium. Pop et al. [2] examined the problem of natural convection heat transfer about cylinders of elliptic cross section in a porous medium. Yih [3] studied the heat and mass transfer from a permeable horizontal cylinder in a fluid-saturated porous medium. Kumari and Jayanthi [4] studied the non-Darcy non-Newtonian natural convection flow over a horizontal cylinder in a porous medium. Cheng [5] studied the heat and mass transfer from a permeable horizontal cylinder of elliptic cross section in a fluid-saturated porous medium.

The thermal non-equilibrium model is used to account for the temperature difference between solid and fluid phases within the representative control volume in porous media. Rees and Pop [6] studied the vertical natural convection boundary-layer flow in a porous medium using a thermal non-equilibrium model. Mohamad [7] studied the natural convection in a differentially heated cavity filled with a saturated porous matrix. Baytas and Pop [8] used a thermal non-equilibrium model to study the natural convection flow in a square porous cavity. Saeid [9] used a thermal non-equilibrium model to study the natural convection near a horizontal cylinder in a porous medium.

This work applies the coordinate transformation and the cubic spline collocation method to analyze the heat transfer by natural convection along a horizontal elliptical cylinder in fluid saturated porous media with constant wall temperature using a thermal non-equilibrium model. The influence of the thermal conductivity ratio parameter, the heat transfer coefficient parameter, and the aspect ratio on the heat transfer characteristics near a horizontal elliptical cylinder in a fluid-saturated porous medium is examined in both cases when the major axis is horizontal (blunt orientation) and vertical (slender orientation).

2 Problem Formulation

Consider the steady laminar natural convection boundary-layer flow driven by temperature gradients near a horizontal cylinder of elliptic cross section

embedded in a homogeneous fluid-saturated porous medium. The coordinate system for the elliptical cylinder with blunt orientation is shown in Fig. 1, where *a* is the length of semi-major axis, *b* is the length of semi-minor axis, *A* represents the angle made by the outward normal from the cylinder with the downward vertical, and *B* is the eccentric angle. For cylinders of elliptic cross section, there are two orientations to consider: the orientation is blunt when the major axis is horizontal, as shown in Fig. 1, and the orientation is slender when the major axis is vertical.

The surface of the cylinder is held at a constant temperature T_w which is higher than the ambient fluid temperature T_∞. The fluid properties are assumed to be constant except for density variations in the buoyancy force term. The viscous drag and inertial terms are neglected. Using the thermal non-equilibrium model and Darcy's law, we can write the governing boundary-layer equations in two-dimensional Cartesian coordinates as [9]

$$\frac{\partial u}{\partial x}+\frac{\partial v}{\partial y}=0 \tag{1}$$

$$u=\frac{gK^* \sin A}{\nu}\beta\left(T_f-T_\infty\right) \tag{2}$$

$$\left(\rho C_p\right)_f\left(u\frac{\partial T_f}{\partial x}+v\frac{\partial T_f}{\partial y}\right)=\varepsilon k_f\frac{\partial^2 T_f}{\partial y^2}+h\left(T_s-T_f\right) \tag{3}$$

$$\left(1-\varepsilon\right)k_s\frac{\partial^2 T_s}{\partial y^2}+h\left(T_f-T_s\right)=0 \tag{4}$$

The appropriate boundary conditions are:

$$v=0,\ T_f=T_w,\ T_s=T_w \text{ on } y=0 \tag{5}$$

$$u=0,\ T_f=T_\infty,\ T_s=T_\infty \text{ as } y\to\infty \tag{6}$$

Here *u* and *v* are the volume-averaged velocity components in the *x* and *y* directions, respectively. T_f and T_s are the fluid-phase and solid-phase temperature, respectively. k_f and k_s are the fluid-phase and solid-phase thermal conductivity, respectively. *h* is the heat transfer coefficient between the solid and fluid phases. Property ν is the kinematic viscosity of the fluid, and *g* is the gravitational acceleration. β is the coefficient of volume expansion. ρ_f and c_{P_f} are the density and constant-pressure specific heat of the fluid, respectively. K^* and ε are the permeability and porosity of the porous medium, respectively.

After introducing the stream function $\overline{\psi}$ to satisfy the relations: $u=\partial\overline{\psi}/\partial y$ and $v=-\partial\overline{\psi}/\partial x$,

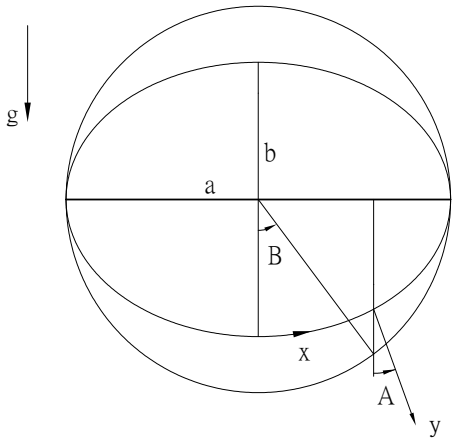

Fig. 1. Physical model and coordinates for an elliptic cylinder of blunt orientation.

we define the nondimensional variables: $\xi=x/a$, $\eta=\left(y/a\right)Ra^{1/2}$, $\psi=\overline{\psi}/\left(\varepsilon\alpha_f Ra^{1/2}\right)$, $\theta_f=\left(T_f-T_\infty\right)/\left(T_w-T_\infty\right)$, $\theta_s=\left(T_s-T_\infty\right)/\left(T_w-T_\infty\right)$, where $Ra=Kg\beta a\left(T_w-T_\infty\right)/\left(\varepsilon\alpha_f\nu\right)$ is the Darcy-Rayleigh number and α_f is the thermal diffusivity of the fluid, Eqs. (1)-(6) become the following equations:

$$\frac{\partial\psi}{\partial\eta}=\theta_f \sin A \tag{7}$$

$$\frac{\partial\psi}{\partial\eta}\frac{\partial\theta_f}{\partial\xi}-\frac{\partial\psi}{\partial\xi}\frac{\partial\theta_f}{\partial\eta}=\frac{\partial^2\theta_f}{\partial\eta^2}+H\left(\theta_s-\theta_f\right) \tag{8}$$

$$\frac{\partial^2\theta_s}{\partial\eta^2}+KH\left(\theta_f-\theta_s\right)=0 \tag{9}$$

The associated boundary conditions are

$$\frac{\partial\psi}{\partial\xi}=0,\ \theta_f=1,\ \theta_s=1 \text{ on } \eta=0 \tag{10}$$

$$\frac{\partial\psi}{\partial\eta}=0,\ \theta_f=0,\ \theta_s=0 \text{ as } \eta\to\infty \tag{11}$$

A further transformation is needed for bodies with rounded lower ends because $\sin A/\xi$ approaches a constant value as ξ approaches zero [2, 10]. The new nondimensional variable is defined as

$$f\left(\xi,\eta\right)=\xi^{-1}\psi \tag{12}$$

Substituting Eq. (12) into Eqs. (7)-(9), we obtain the following boundary-layer governing equations:

The resulting dimensionless governing equations become the following equations:

$$f'=\frac{\sin A}{\xi}\theta_f \tag{13}$$

$$\theta_f'' + f\theta_f' = \xi\left(f' \frac{\partial \theta_f}{\partial \xi} - \theta_f' \frac{\partial f}{\partial \xi} \right) - H\left(\theta_s - \theta_f\right) \quad (14)$$

$$\theta_s'' + KH\left(\theta_f - \theta_s\right) = 0 \quad (15)$$

The boundary conditions are

$$f = 0,\ \theta_f = 1,\ \theta_s = 1 \text{ on } \eta = 0 \quad (16)$$

$$f' = 0,\ \theta_f = 0,\ \theta_s = 0 \text{ as } \eta \to \infty \quad (17)$$

Note that primes denotes partial derivation with respect to η. Moreover, the thermal conductivity ratio parameter and the heat transfer coefficient parameter are respectively defined as $K = \left(\varepsilon k_f\right) / \left[(1-\varepsilon)k_s\right]$ and $H = \left(ha^2\right) / \left(\varepsilon k_f Ra\right)$.

Here ξ and $\sin A$ can be given in terms of the eccentric angle B by the relations:

(1) For blunt orientation:

$$\xi = \int_0^B \left(1 - e^2 \sin^2 \gamma\right)^{1/2} d\gamma \quad (18)$$

$$\sin A = \frac{b}{a} \frac{\sin B}{\left(1 - e^2 \sin^2 B\right)^{1/2}} \quad (19)$$

(2) For slender orientation:

$$\xi = \int_0^B \left(1 - e^2 \cos^2 \gamma\right)^{1/2} d\gamma \quad (20)$$

$$\sin A = \frac{\sin B}{\left(1 - e^2 \cos^2 B\right)^{1/2}} \quad (21)$$

where e denotes the eccentricity expressed as $e = \left(1 - b^2/a^2\right)^{1/2}$ and b/a is the aspect ratio of the elliptic cylinder.

When ξ approaches zero, as shown in Eqs. (18)-(21), the value of $\sin A/\xi$ approaches the aspect ratio b/a for the elliptic cylinder with blunt orientation. Moreover, the value of $\sin A/\xi$ approaches the value of a^2/b^2 for the elliptic cylinder with slender orientation as ξ approaches zero.

The local Nusselt number for the fluid can be written as

$$\frac{Nu_f}{Ra^{1/2}} = -\theta_f'(\xi, 0) \quad (22)$$

The local Nusselt number for the solid matrix can be given by

$$\frac{Nu_s}{Ra^{1/2}} = -\theta_s'(\xi, 0) \quad (23)$$

The local Nusselt number for the porous medium can be expressed as

$$\frac{Nu}{Ra^{1/2}} = \frac{1}{K+1}\left[-K\theta_f'(\xi, 0) - \theta_s'(\xi, 0)\right] \quad (24)$$

Table 1. The value of $F_{i,j}$, $G_{i,j}$, and $S_{i,j}$.

θ_f	$F_{i,j}$	$\left(\theta_f\right)_{i,j}^n + \Delta\tau\left[-\xi_i l_f^n \left(\frac{\partial \theta_f}{\partial \xi}\right)_{i,j}^n\right] + \Delta\tau H\left[\left(\theta_s\right)_{i,j}^n - \left(\theta_f\right)_{i,j}^n\right]$
	$G_{i,j}$	$\Delta\tau\left[f_{i,j}^n + \xi_i \left(\frac{\partial f}{\partial \xi}\right)_{i,j}^n\right]$
	$S_{i,j}$	$\Delta\tau$
θ_s	$F_{i,j}$	$\left(\theta_s\right)_{i,j}^n + \Delta\tau KH\left[\left(\theta_f\right)_{i,j}^n - \left(\theta_s\right)_{i,j}^n\right]$
	$G_{i,j}$	0
	$S_{i,j}$	$\Delta\tau$

Table 2. Comparison of values of $Nu/\sqrt{Ra}$ for $b/a = 1$ between the present results with the solutions reported by Merkin [1] and Yih [3].

ξ	Merkin [1]	Yih [3]	Present results
0	0.6276	0.6276	0.6276
0.2	0.6245	0.6245	0.6245
0.6	0.5996	0.5996	0.5997
1.0	0.5508	0.5508	0.5510
1.4	0.4800	0.4800	0.4804
1.8	0.3901	0.3899	0.3904
2.2	0.2847	0.2843	0.2849
2.6	0.1679	0.1677	0.1680
3.0	0.0444	0.0446	0.0444

3 Problem Solution

The governing differential equations, Eqs. (14) and (15), and the boundary conditions, Eqs. (16) and (17), can be solved by the cubic spline collocation method [11, 12]. The Simpson's rule for variable grids is used to calculate the value of *f* at every position from Eq. (13) and the boundary conditions, Eqs. (16) and (17). Variable grids with 200 grid points are used in the η direction. The minimum step size is 0.01. The value of the edge of the boundary ayer η_∞ is about 12. Moreover, a grid with 150 grid points is used in the ξ direction. At every grid point, the iteration process continues until the convergence criterion for all the

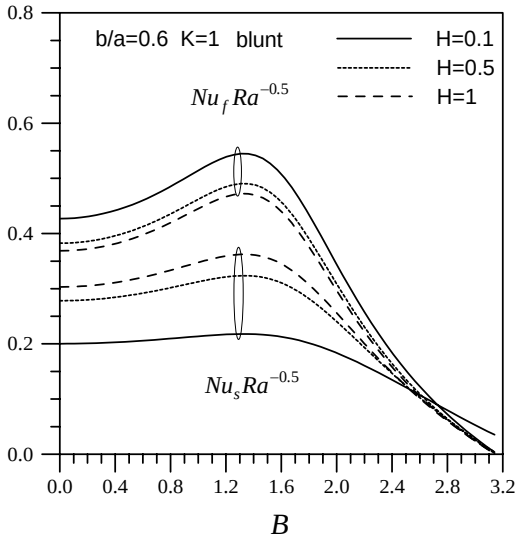

Fig. 2. Effects of heat transfer coefficient parameter on the local Nusselt number for the fluid and solid phases.

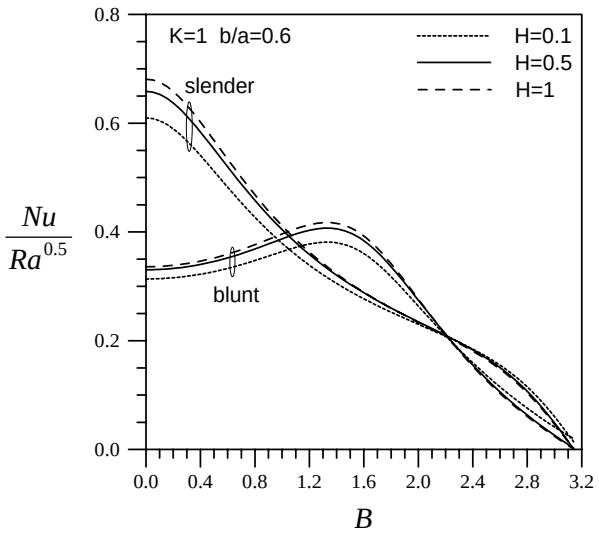

Fig. 4. Effects of heat transfer coefficient parameter on the local Nusselt number for the porous medium.

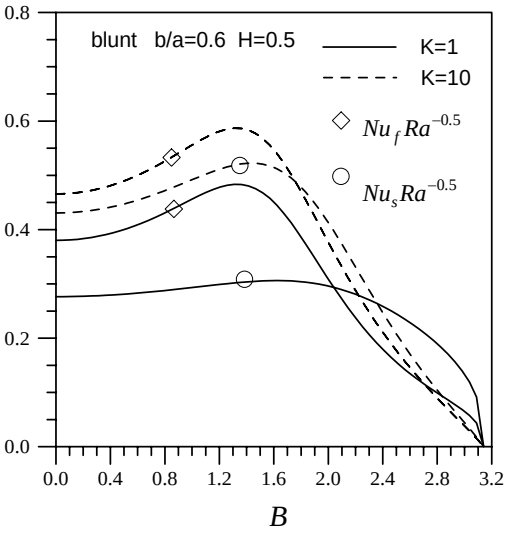

Fig. 3. Effects of thermal conductivity ratio parameter on the local Nusselt number for the fluid and solid phases.

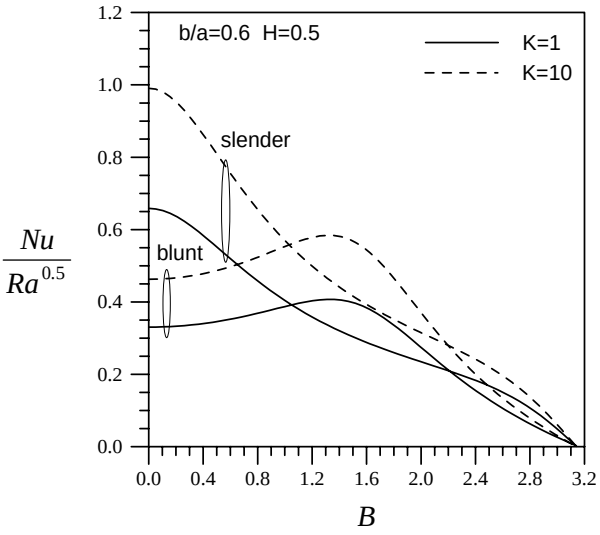

Fig. 5. Effects of thermal conductivity ratio parameter on the local Nusselt number for the porous medium.

variables, 10^{-6}, is achieved. The present calculation for Eqs. (13)-(17) can be performed from the bottom up to the top of the elliptic cylinder. Eqs. (14) and (15) can be discretized by using the false transient technique and the cubic spline collocation method [11, 12] as

$$\frac{(\theta_f)_{i,j}^{n+1}-(\theta_f)_{i,j}^{n}}{\Delta\tau}+\xi_i l_f^n\left(\frac{\partial\theta_f}{\partial\xi}\right)_{i,j}^{n}-\xi_i l_{\theta_f}^{n+1}\left(\frac{\partial f}{\partial\xi}\right)_{i,j}^{n}$$
$$=L_{\theta_f}^{n+1}+f_{i,j}^{n}l_{\theta_f}^{n+1}+H\left[(\theta_s)_{i,j}^{n}-(\theta_f)_{i,j}^{n}\right] \quad (25)$$

$$\frac{(\theta_s)_{i,j}^{n+1}-(\theta_s)_{i,j}^{n}}{\Delta\tau}=L_{\theta_s}^{n+1}+KH\left[(\theta_f)_{i,j}^{n}-(\theta_s)_{i,j}^{n}\right] \quad (26)$$

where

$\Delta\xi=\xi_i-\xi_{i-1}$, $\Delta\eta=\eta_i-\eta_{i-1}$

$$\left(\frac{\partial\vartheta}{\partial\xi}\right)_{i,j}=\frac{\vartheta_{i,j}-\vartheta_{i,j-1}}{\Delta\xi_i} \text{ for } i=1$$

$$\left(\frac{\partial\vartheta}{\partial\xi}\right)_{i,j}=\frac{-3\vartheta_{i,j}+4\vartheta_{i,j-1}-\vartheta_{i,j-2}}{2\Delta\xi_i} \text{ for } i\geq 2$$

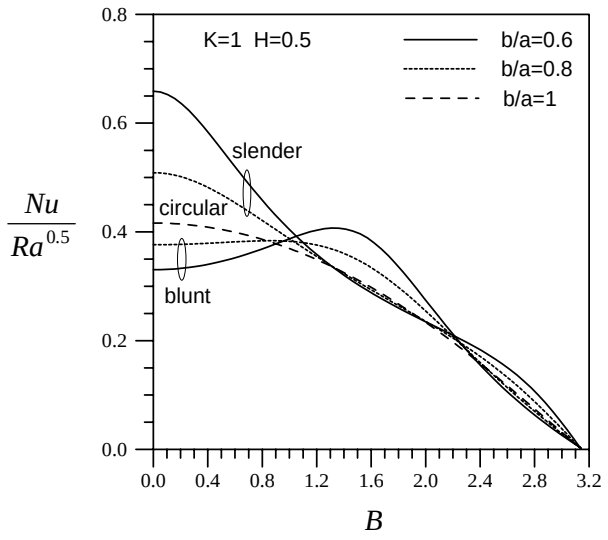

Fig. 6. Effects of aspect ratio on the local Nusselt number for the porous medium.

$$l_\phi = \frac{\partial \vartheta}{\partial \eta},\ L_\phi = \frac{\partial^2 \vartheta}{\partial \eta^2} \tag{27}$$

Note that ϑ refers to θ_f and θ_s, and the quantity $\Delta\tau = \tau^{n+1} - \tau^n$ represents the false time step.

After some arrangement, Eqs. (25) and (26) can be written in the following spline approximation form:

$$\vartheta_{i,j}^{n+1} = F_{i,j} + G_{i,j} l_{\vartheta_{i,j}}^{n+1} + S_{i,j} L_{\vartheta_{i,j}}^{n+1} \tag{28}$$

The quantities *F*, *G*, and *S* are known coefficients evaluated at previous time steps (Table 1). By using the cubic spline relations [11, 12], Eq. (28) may be written in the following tridiagonal form as

$$A_{i,j}\vartheta_{i,j-1} + B_{i,j}\vartheta_{i,j} + C_{i,j}\vartheta_{i,j+1} = D_{i,j} \tag{29}$$

Here Eq. (29) can be easily solved by using the Thomas algorithm.

In order to check the accuracy of the present method, the local Nusselt number $Nu/Ra^{0.5}$ for $b/a = 1$ obtained in the current study under Darcian assumptions for a horizontal circular cylinder are compared with the solutions reported by Merkin [1] and Yih [3] by using the thermal-equilibrium model. As shown in Table 2, the present results are found to be in excellent agreement with the results of Merkin [1] and Yih [3].

Fig. 2 plots the variation of the local Nusselt number for the fluid and solid phases, $Nu_f / Ra^{0.5}$ and $Nu_s / Ra^{0.5}$, with the eccentric angle *B* of the elliptical cylinder for various heat transfer coefficient parameters ($H = 0.1$, 0.5, and 1), *K*=1, and *b/a*=0.6 and the elliptical cylinder with blunt orientation. Comparing the curves in Fig. 2, we can deduce that increasing the heat transfer coefficient parameter tends to decrease the difference between the local Nusselt number of the fluid and solid phases in porous media. As the heat transfer coefficient parameter increases, the local Nusselt number for the fluid phase is decreased while the local Nusselt number for the solid phase is increased

Fig. 3 plots the variation of the local Nusselt number for the fluid and solid phases, $Nu_f / Ra^{0.5}$ and $Nu_s / Ra^{0.5}$, with the eccentric angle *B* of the elliptical cylinder for various thermal conductivity ratio parameters ($K = 1$ and 10), *H*=0.5, and *b/a*=0.6 and the elliptic cylinder with blunt orientation. The Nusselt number for the fluid phase is always higher than that for solid phase for given values of heat transfer coefficients and thermal conductivities; thus major part of heat transfer is taken place in the fluid phase. Moreover, increasing the thermal conductivity ratio parameter tends to decrease the difference between the local Nusselt number of the fluid and solid phases in porous media. The local Nusselt numbers for the fluid and solid phases in porous media increase with an increase in the thermal conductivity ratio parameter.

Fig. 4 plots the variation of the local Nusselt number for the porous medium $Nu/Ra^{0.5}$ with the eccentric angle *B* of the elliptical cylinder for various heat transfer coefficient parameters ($H = 0.1$, 0.5, and 1), *K*=1, and *b/a*=0.6. For the elliptical cylinder with blunt orientation, the local Nusselt number first increases with distance from the stagnation point, reaches a maximum, and then decreases to zero at the top of the elliptical cylinder. For an elliptical cylinder with slender orientation, the local Nusselt number decreases monotonically from the lower end of the cylinder to the upper end of the cylinder; that is due to the increase in boundary layer thickness. Moreover, comparing the curves in Fig. 4, we can deduce that increasing the heat transfer coefficient parameter tends to increase the heat transfer rates between the porous medium and the wall.

Fig. 5 shows the local Nusselt number for the porous medium $Nu/Ra^{0.5}$ as functions of the eccentric angle *B* of the elliptical cylinder for various thermal conductivity ratio parameters ($K = 1$ and 10), *H*=0.5, and *b/a*=0.6. Comparing the curves in Fig. 5, we can deduce that increasing the thermal conductivity ratio parameter tends to increase the heat transfer rates between the porous medium and the wall.

Fig. 6 shows the local Nusselt number for the porous medium $Nu/Ra^{0.5}$ as a function of the

eccentric angle B of the elliptical cylinder for various aspect ratios (b/a=0.6, 0.8, and 1), H=0.5, and K=1. The total heat transfer rates of the elliptic cylinder with slender orientation are higher than those of the elliptical cylinder with blunt orientation for any aspect ratio b/a smaller than one. When the aspect ratio b/a is increased (i.e., the eccentricity is decreased), the total heat transfer rates for the elliptic cylinder of slender orientation tend to decrease while those for the elliptic cylinder of blunt orientation tend to increase, and finally the total heat transfer rates of slender orientation equal to those of blunt orientation when the aspect ratio b/a equals to one. Therefore, the elliptic cylinders of slender orientation are found to be superior to the elliptic cylinders of blunt orientation from the viewpoint of the total heat transfer rates in fluid-saturated porous media.

4 Conclusion

Natural convection heat transfer from a horizontal cylinder with elliptic cross section in porous media has been studied by using a thermal non-equilibrium model. Here a coordinate transformation is employed to transform the governing equations into nondimensional nonsimilar boundary layer equations. The obtained boundary layer equations are then solved by the cubic spline collocation method. The effects of the heat transfer coefficient, thermal conductivity ratio, and the aspect ratio on the Nusselt numbers for the elliptical cylinders of blunt and slender orientations in porous media have been studied. The results show that increasing the porosity scaled thermal conductivity ratio or the heat transfer coefficient between the solid and fluid phases tends to increase the heat transfer rates. Moreover, the heat transfer rates between the porous medium and the surface for the elliptical cylinder with slender orientation are higher than those with blunt orientation.

Acknowledgements

This work was supported by National Science Council of Republic of China under the grant no. NSC 95-2221-E-218-058.

References:

[1] J.H. Merkin, Free Convection Boundary Layers on Axi-Symmetric and Two-Dimensional Bodies of Arbitrary Shape in a Saturated Porous Medium, *International Journal of Heat and Mass Transfer*, Vol. 22, 1979, pp. 1461-1462.

[2] I. Pop, M. Kumari, G. Nath, Free Convection about Cylinders of Elliptic Cross Section Embedded in a Porous Medium, *International Journal of Engineering Sciences*, Vol. 30, 1992, pp. 35-45.

[3] K.A. Yih, Coupled Heat and Mass Transfer by Natural Convection Adjacent to a Permeable Horizontal Cylinder in a Saturated Porous Medium, *International Communications in Heat and Mass Transfer*, Vol. 26, 1999, pp. 431-440.

[4] M. Kumari, S. Jayanthi, Non-Darcy Non-Newtonian Free Convection Flow over a Horizontal Cylinder in a Saturated Porous Medium, *International Communications in Heat and Mass Transfer*, Vol. 31, 2004, pp. 1219-1216.

[5] C.Y. Cheng, Nonsimilar Solutions for Natural Convection Heat and Mass Transfer near a Permeable Horizontal Cylinder of Elliptic Cross Section in Porous Media, *WSEAS Transactions on Mathematics*, Vol. 5, 2006, pp. 1095-1101.

[6] D.A.S. Rees, I. Pop, Vertical Free Convective Boundary-Layer Flow in a Porous Medium Using a Thermal Non-Equilibrium Model, *Journal of Porous Media*, Vol. 3, 2000, pp. 31-44.

[7] A.A. Mohamad, Non-Equilibrium, Natural Convection in a Differentially Heated Cavity Filled with a Saturated Porous Matrix, *ASME Journal of Heat Transfer*, Vol. 122, 2000, pp. 380-384.

[8] A.C. Baytas, I. Pop, Free Convection in a Square Porous Cavity Using a Thermal Non-Equilibrium Model, *International Journal of Thermal Sciences* , Vol. 41, 2002, pp. 861-870.

[9] N.H. Saeid, Analysis of Free Convection about a Horizontal Cylinder in a Porous Media Using a Thermal Non-Equilibrium Model, *International Communications in Heat and Mass Transfer*, Vol. 33, 2006, pp. 158-165.

[10] J.H. Merkin, Free Convection Boundary Layers on Cylinders of Elliptic Cross Section, *ASME Journal of Heat Transfer*, Vol. 99, 1977, pp. 453-457.

[11] S.G. Rubin, R.A. Graves, Viscous Flow Solution with a Cubic Spline Approximation, *Computers and Fluids*, Vol. 3, 1975, pp. 1-36.

[12] P. Wang, R. Kahawita, Numerical Integration of Partial Differential Equations Using Cubic Spline, *International Journal of Computer Mathematics*, Vol. 13, 1983, pp. 271-286.